

ELECTROSTATICS OF NANOWIRES AND NANOTUBES: APPLICATION FOR FIELD-EFFECT DEVICES

ALEXANDER SHIK, HARRY E. RUDA

*Centre for Advanced Nanotechnology, University of Toronto,
Toronto M5S 3E4, Canada*

SLAVA V. ROTKIN[†]

*Physics Department, Lehigh University,
16 Memorial Drive East, Bethlehem, PA 18015, USA*

[†]*rotkin@lehigh.edu*

Received (received date)

Revised (revised date)

Accepted (accepted date)

We present a quantum and classical theory of electronic devices with one-dimensional (1D) channels made of a single carbon nanotube or a semiconductor nanowire. An essential component of the device theory is a self-consistent model for electrostatics of 1D systems. It is demonstrated that specific screening properties of 1D wires result in a charge distribution in the channel different from that in bulk devices. The drift-diffusion model has been applied for studying transport in a long channel 1D field-effect transistor. A unified self-consistent description is given for both a semiconductor nanowire and a single-wall nanotube. Within this basic model we analytically calculate equilibrium (at zero current) and quasi-equilibrium (at small current) charge distributions in the channel. Numerical results are presented for arbitrary values of the driving current. General analytic expressions, found for basic device characteristic, differ from equations for a standard bulk three-dimensional field-effect device. The device characteristics are shown to be sensitive to the gate and leads geometry and are analyzed separately for bulk, planar and quasi-1D contacts. The basic model is generalized to take into account external charges which can be polarized and/or moving near the channel. These charges change the self-consistent potential profile in the channel and may show up in device properties, for instance, a hysteresis may develop which can have a memory application.

Keywords: electrostatics of low-dimensional systems; device physics; nanotube and nanowire transistors.

1. Introduction

A basic trend in modern electronics is the wider device application of nanostructures, having at least one geometric size a less than some characteristic electron length: de Broglie wavelength λ , electron mean free path l_{tr} , or Debye screening radius r_s . For $a \sim \lambda$ the electronic properties of nanostructures are strongly modified by size quantization of the energy spectrum, while for $a < l_{tr}$ transport acquires bal-

listic character. Influence of these two phenomena on the characteristics of various low-dimensional devices has been widely discussed in the literature. In the present paper, partially based on our short communication ¹, we consider modification of the screening phenomena in nanowires and nanotubes with the radius a less than r_s and apply this knowledge to the problem of a field-effect transistor (FET) based on these quasi-one-dimensional (quasi-1D) nanostructures.

All low-dimensional systems are characterized by dramatic suppression of electron screening as compared to bulk semiconductors. Therefore, a different theoretical approach has to be used for the calculation of a screened potential ϕ . In bulk materials, $\phi(\mathbf{r})$ is found from the Poisson equation where the induced charge is proportional to the Laplacian (second derivative) of ϕ . In low-dimensional systems, for determination of $\phi(\mathbf{r})$ one should solve the Laplace, rather than Poisson, equation containing the screening charge in boundary conditions. For two-dimensional electrons (see, e.g., ²) the surface charge density is proportional to the field, the first derivative of potential. Similar dimensional analysis for quasi-1D nanowires ³ shows that for slow charge and potential variations (with the characteristic length $l \gg a$), the one-dimensional charge density $\eta(x)$ is simply proportional to local value of an induced potential at the nanowire surface:

$$\phi^{ind}(x, a) \simeq \frac{2}{\varepsilon} \ln \left(\frac{l}{a} \right) \eta(x) \quad (1)$$

where ε is the dielectric constant of the medium outside nanowire. The weak screening in 1D case is due to the fact that any charge in a system creates electric field in the whole environment, including both the wire and the surrounding medium, while the carriers responsible for screening are severely restricted in their motion to one single direction along the wire. This differs drastically from bulk semiconductors with carriers present in all points where electric field exists and providing effective screening by re-distributing in this field.

On the basis of Eq.(1) a self-consistent electrostatics of quasi-1D systems can be easily formulated and used for modelling of a number of 1D applications, including transport and memory devices ^{1,4}, optics ⁵, nanoelectromechanical systems ⁶, and even artificial ion channels ⁷. In the present paper we restrict ourselves to electronics applications.

The paper proceeds as follows. Sec.2 presents the basic equations to be solved to calculate the charge density and current in 1D FET. Sec.3 gives a solution of these equations for the case of bulk electrodes. We show in Sec.4 that an analytical treatment of the model is possible at low drain voltage. The next section presents numerical results for an arbitrary drain voltage, that are given separately for Ohmic and injecting contacts in Sec.5.1 and 5.2 respectively. In this part of the paper we closely follow our earlier results (published in ^{1,4}), which review is needed to emphasize on the role of the contact geometry in last two sections. Though, it follows from the general expressions of Sec.2 that the potential profile along the channel is a function of the contact geometry, in this paper we add new evidence for this. Sec.6

deals with the cases of 2D and 1D contacts, presenting for the first time analytical expressions for equilibrium charge distribution and, thus, transconductance of the 1D FET. Last section reviews the role of the charge injected into the substrate and gives a description for the hysteresis in a real 1D FET structure.

2. Formulation of the problem: Device geometry

We consider a 1D FET in which the channel is a semiconductor nanowire or a carbon nanotube. The schematic geometry of such FET is shown in Fig.1. The structure includes the source ($x < -L/2$) and drain ($x > L/2$) electrodes (in our model they are assumed to be identical) connected by a nanowire of the length L . The gate electrode is separated by a thin dielectric layer of the thickness d . We assume the wire to be uniformly doped with the linear concentration $N = \text{const}(x)$ (in pristine nanotubes $N = 0$). In the absence of source-drain voltage the equilibrium carrier concentration in the channel has some symmetric profile $n_0(x)$, which may differ from N and be coordinate-dependent. This profile is due to the contact potentials between the channel and electrodes determined by their work function difference, any electric potential induced by charges in the environment (in particular, movable charges), and the gate voltage V_g . When the structure is in operation, the source-drain voltage V_d causes a current j along the channel and thus a re-distribution of carrier concentration as compared with $n_0(x)$. The voltage V_g (and also the potential of the variable charge in the environment, which is presented in the case of a nanotube nonvolatile memory, for example ^{26,27,28}) changes the concentration in a channel controlling the FET transport. We employ the drift-diffusion model in this paper and assume that the scattering rate in the channel is sufficiently high to support a local charge equilibrium assumption. This is likely valid for the most of the nanowire FETs and, at least, for some of nanotube devices. In the opposite (ballistic) limit, discussed in ⁸, the channel and contact geometry influences the device characteristics via lowering the tunnel barriers at the source and/or drain. Nevertheless, the device electrostatics is one of the most important factors for the total conductance. In this work we restrict ourselves to the case of drift-diffusion transport when the modulation of the channel conductance is determinant for the transport through the whole device.

We measure all potentials from the middle point of the wire ($x = 0$) so that the source and drain potentials are $-V_d/2$ and $V_d/2$. In this case the potentials along the wire and concentration changes caused by V_g together with the contact potentials and by V_d are, respectively, symmetric and antisymmetric functions of x and will be denoted by the subscripts s and a : $\phi_{s,a}(x)$ and $n_{s,a}(x)$. The potential of any external charges, movable or not, has no specific symmetry. This is a random function of x and has to be averaged over the distribution of the charge centers (a possible averaging procedure for 2D charge impurities can be found in ⁹). Since the movable charges in the environment obey the same electrostatics as the movable charges in the tube, it is rational to assume that their potential, on average, will

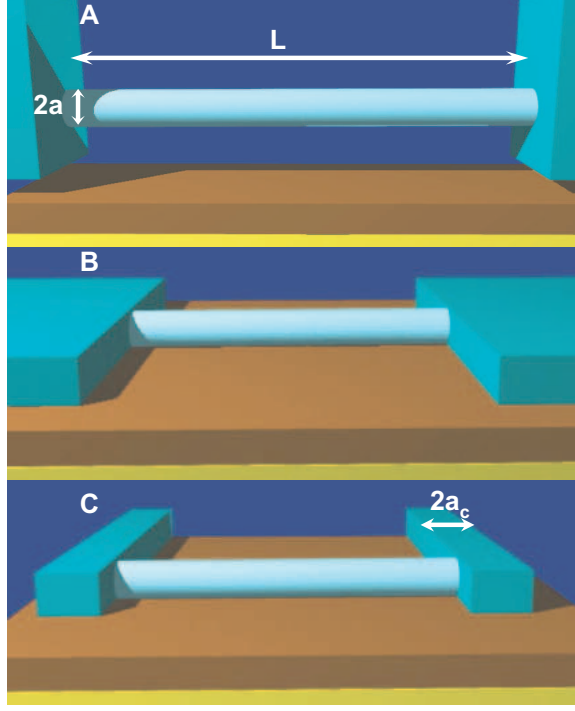


Figure 1: Possible geometry of contacts to a 1D FET: (A) 3D contacts (all dimensions are much larger than the channel width), (B) 2D contacts and (C) 1D contacts. The potential profile along the weakly screening 1D channel depends on the dimension (and other geometry) of the contacts, which results in a different device behavior.

have also a similar coordinate dependence as the total electrostatic potential. For the sake of clarity, in the most part of the paper, except for Sec.7, no external movable/polarizable charge will be considered.

The potentials $\phi_{s,a}(x)$ can be divided into two parts: the components $\phi_{s,a}^0(x)$ created by electrodes and contact potentials, which should be found from the Laplace equation containing no wire charge, and the components $\phi_{s,a}^1(x)$ caused by the electron charge in a wire $-en_{s,a}(x)$. We assume that the characteristic lengths L and d determining the potential and concentration distribution along the wire, exceed noticeably the wire radius a . In this case the relationship between $\phi_{s,a}^1(x)$ and $\rho(x)$ is given by the linear formula Eq.(1). Using this relationship, the current j containing both drift and diffusion components* can be written for a semiconductor nanowire

*Contrary to three- and two-dimensional electron systems where the role of diffusion current at the distances much larger than the screening length is negligible, in quasi-one-dimensional electron systems its contribution is parametrically the same as that of drift current caused by ϕ^1 and cannot be ignored.

with non-degenerate carriers in the form ¹⁰:

$$\frac{j}{e\mu} = n(x) \frac{d\phi^0}{dx} - \left[\frac{2e}{\varepsilon} \ln \left(\frac{l}{a} \right) n(x) + \frac{kT}{e} \right] \frac{dn}{dx} \quad (2)$$

where $n = n_s + n_a$, $\phi^0 = \phi_s^0 + \phi_a^0$, μ is the carrier mobility, and the characteristic length of charge variation along the wire l in our case has the order of $\min\{L, 2d\}$. For a nanotube with $N = 0$ and degenerate carriers, kT should be replaced by the concentration-dependent Fermi energy and, instead of Eq.(2), we have ^{11,12}:

$$\frac{j}{e\mu} = n(x) \frac{d\phi^0}{dx} - eC_t^{-1} n(x) \frac{dn}{dx}, \quad (3)$$

where C_t^{-1} is the inverse capacitance of the nanotube derived in ¹¹ and containing both logarithmic geometrical capacitance similar to Eq.(2) and the quantum capacitance of the 1D electron gas, $1/(e^2\nu) \simeq 0.31$ for one degenerate subband of a single wall nanotube with the density of states ν .

Eq.(3) is easier to solve than Eq.(2) and in this connection it is important to note that at some conditions the latter can be also reduced to a simpler form. It can be easily shown that at $A \equiv (2e^2N/\varepsilon kT) \ln(l/a) \gg 1$ the last term in Eq.(2) can be neglected and it acquires the form of Eq.(3) with $C_t^{-1} = (2/\varepsilon) \ln(l/a)$. This has a rather simple explanation. Two terms in the square brackets in Eq.(2) correspond, respectively, to drift in a self-consistent electric field and to diffusion. In degenerate nanotubes these terms have exactly the same appearance and may be written as a single term with the coefficient C_t^{-1} . In a non-degenerate system the terms are different but for $A \gg 1$ the diffusion term can be neglected.

We will solve the first order differential equation for $n(x)$ given by Eq.(2) or (3), with the boundary conditions

$$n(\pm L/2) = n_c \quad (4)$$

assuming the source and drain to support constant concentration at the contacts, independent of the applied voltage. The two conditions Eq.(4) allow us to determine the integration constant and the value of current j so far considered as some unknown constant.

Depending on the relationship between n_c and N , three possible situations can be realized. The condition $n_c = N$ corresponds to ideal Ohmic contacts not disturbing electric properties of a wire, $n_c > N$ describes the situation where the carriers are provided by electrodes, which is often the case for nanotubes, and $n_c < N$ corresponds to depleted Schottky contacts. In the latter case, the regions near contacts have the lowest carrier concentration and determine the current through the structure. At the same time, this concentration is fixed by Eq.(4) and does not depend on V_g . As a result, for the structures adequately described by the classical drift-diffusion theory (see Eq.(2)), transconductance will be very small. The only possible situation of an applied interest is that when the Schottky barrier has a

noticeable tunnel transparency strongly dependent on V_g . This situation has been thoroughly considered in ^{8,13} and will not be discussed below.

3. Potential profile: 3D bulk electrodes

The first step in calculating characteristics of a particular FET consists in finding the potential profile $\phi^0(x)$ along the channel. For $n_c = N$ it can be done by direct solution of the Laplace equation determining the potential $\Phi(x, y)$ created by the given system of electrodes.[†] However, for $n_c \neq N$ the basic formulae of the previous section require some modification. In the closest vicinity of contacts there exists a finite charge density $e(N - n_c)$ in a wire. To provide equipotentiality of metallic contacts, we must assume the presence of charges of the opposite sign (image charges) just beyond the contacts. This means discontinuity of charge density at $x = \pm L/2$ and makes doubtful the adequacy of Eq.(1) assuming smooth charge and potential variations. To avoid this difficulty, we will measure n from n_c by assuming in Eq.(2) $n(x) = n_c + \Delta n(x)$. In this case, the boundary conditions Eq.(4) are replaced by

$$\Delta n(\pm L/2) = 0 \quad (5)$$

but the potential acquires an additional term $\phi_c(x)$:

$$\phi_s^0(x) = \phi_c(x) + \phi_g(x) \quad (6)$$

where $\phi_g(x)$, as earlier, is determined by the gate, source and drain electrodes at $V_d = 0$ while $\phi_c(x)$ is a potential of a wire with uniform charge $e(N - n_c)$ between metallic contacts at $x = \pm L/2$. This is just the charge which, together with its images, may have discontinuities at the contacts.

In this section we calculate $\phi^0(x)$ for the case of bulk contacts representing metallic or heavily doped semiconductor regions with all three dimensions considerably exceeding the characteristic lengths a, d and L . In this case the contact size can be assumed infinite as it is shown in Fig.1A. Exact calculations are rather cumbersome and to obtain relatively simple analytical results, we make some additional approximation. Let us assume that the relation $d \ll L$, often realized in 1D FETs, is fulfilled in our system as well. In this case the potential distribution in the most part of inter-electrode space will not noticeably change if we neglect the dielectric-filled slit of the thickness d between the channel and the gate. In other words, we solve the Laplace equation $\Delta\Phi = 0$ in the semi-infinite strip $-L/2 < x < L/2$; $y > 0$ with the boundary conditions: $\Phi(y = 0) = V_g$; $\Phi(x = \pm L/2) = \pm V_d/2$ and then, assuming $y = d$ and adding the expression for $\phi_c(x)$ derived in ¹⁰, obtain the following formulae for $\phi_{s,a}^0(x)$:

[†]Here and henceforth $\Phi(x, y)$ represents the complete solution of the Laplace equation whereas $\phi(x) \equiv \Phi(x, d)$ is the potential along the wire.

$$\begin{aligned}\phi_s^0(x) &= \phi_c(x) + \phi_g(x) = \frac{8e(N - n_c)L}{\pi^2 \varepsilon a} \\ &\times \sum_{n=0}^{\infty} \frac{(-1)^n}{(2n+1)^2} \frac{\{K_0[\frac{\pi a}{L}(2n+1)] - K_0[\frac{2\pi d}{L}(2n+1)]\}}{K_1[\frac{\pi a}{L}(2n+1)]} \cos\left[\frac{\pi x(2n+1)}{L}\right] \\ &+ \frac{4V_g}{\pi} \sum_{n=0}^{\infty} \frac{(-1)^n}{(2n+1)} \cos\left[\frac{\pi x(2n+1)}{L}\right] \exp\left[-\frac{\pi d(2n+1)}{L}\right];\end{aligned}\quad (7)$$

$$\phi_a^0(x) = V_d \left[\frac{x}{L} + \sum_{n=1}^{\infty} \frac{(-1)^n}{\pi n} \sin\left(\frac{2\pi x n}{L}\right) \exp\left(-\frac{2\pi d n}{L}\right) \right] \quad (8)$$

where K_0 and K_1 are Bessel functions of an imaginary argument¹⁴.

4. Linear conductivity and transconductance

Now we can calculate the carrier concentration Δn and the electric current j caused by the driving voltage V_d . The problem is relatively simple if we restrict ourselves to the linear case by assuming V_d to be sufficiently small. In the zeroth approximation $j = 0$ and both $\phi^0(x)$ and $n(x)$ contain only a symmetric component and are the same as in equilibrium: $\phi_s^0(x) = \phi_c(x) + \phi_g(x)$, $n_s(x) = n_c + \Delta n_0(x)$ where the equation for $\Delta n_0(x)$ is:

$$[n_c + \Delta n_0(x)] \frac{d\phi_s^0}{dx} - \left\{ \frac{2e}{\varepsilon} \ln\left(\frac{l}{a}\right) [n_c + \Delta n_0(x)] + \frac{kT}{e} \right\} \frac{d(\Delta n_0)}{dx} = 0. \quad (9)$$

Direct integration of Eq.(9) with the boundary conditions Eq.(5) transforms it into an algebraic equation for Δn_0 :

$$\ln\left(1 + \frac{\Delta n_0(x)}{n_c}\right) + \frac{2e^2}{\varepsilon kT} \ln\left(\frac{l}{a}\right) \Delta n_0(x) = \frac{e\phi_s^0(x)}{kT}. \quad (10)$$

For degenerate carriers in a nanotube (or for $A \gg 1$), the problem is much simpler since, according to Eq.(3), $\Delta n_0(x)$ is proportional to $\phi_s^0(x)$:

$$\Delta n_0(x) = C_t \phi_s^0(x). \quad (11)$$

We emphasize that Eqs.(2),(3) were derived in the drift-diffusion approximation. On the contrary, the expressions of this section, being equilibrium, remain adequate beyond the drift-diffusion model.

To the first order in V_d , the differential equations (2),(3) can be linearized in n_a . The equation for a nanowire reads as:

$$\begin{aligned}& \left[\frac{2e}{\varepsilon} \ln\left(\frac{l}{a}\right) [n_c + \Delta n_0(x)] + \frac{kT}{e} \right] \frac{dn_a}{dx} + \left[\frac{2e}{\varepsilon} \ln\left(\frac{l}{a}\right) \frac{d(\Delta n_0)}{dx} - \frac{d\phi_s^0}{dx} \right] n_a(x) \\ &= [n_c + \Delta n_0(x)] \frac{d\phi_a^0}{dx} - \frac{j}{e\mu}.\end{aligned}\quad (12)$$

Since $\phi_a^0(x)$ is proportional to V_d , both $n_a(x)$ and j are also linear in V_d . Eq.(12), being solved with the conditions $n_a(0) = n_a(L/2) = 0$, gives the current-induced change of concentration profile $n_a(x)$ and the implicit expression for the current j :

$$\int_0^{L/2} \exp \left[\int_0^x \frac{\left[\frac{2e}{\varepsilon} \ln \left(\frac{l}{a} \right) \frac{d(\Delta n_0)}{dx'} - \frac{d\phi_s^0}{dx'} \right] dx'}{\frac{2e}{\varepsilon} \ln \left(\frac{l}{a} \right) [n_c + \Delta n_0(x')] + \frac{kT}{e}} \right] \frac{\left[[n_c + \Delta n_0(x)] \frac{d\phi_a^0}{dx} - \frac{j}{e\mu} \right] dx}{\frac{2e}{\varepsilon} \ln \left(\frac{l}{a} \right) [n_c + \Delta n_0(x)] + \frac{kT}{e}} = 0. \quad (13)$$

The resulting j depends on the gate voltage V_g through the functions $\phi_s^0(x)$ and $\Delta n_0(x)$, which allows us to calculate the transistor transconductance $s = dj/dV_g$.

For $A \gg 1$ the problem is essentially simplified and, as it has been already mentioned, this case coincides with that for a degenerate nanotube. Instead of Eq.(12), we have:

$$C_t^{-1} [n_c + \Delta n_0(x)] \frac{dn_a}{dx} = [n_c + \Delta n_0(x)] \frac{d\phi_a^0}{dx} - \frac{j}{e\mu} \quad (14)$$

which gives us directly

$$n_a(x) = C_t \left\{ \phi_a^0(x) + \frac{V_d}{2} - \frac{j}{e\mu} \int_{-L/2}^x \frac{dx'}{[n_c + \Delta n_a(x')] } \right\} \quad (15)$$

where

$$j = \frac{V_d}{R}, \quad R = \frac{2}{e\mu} \int_0^{L/2} \frac{dx}{[n_c + \Delta n_0(x)]}. \quad (16)$$

The last expression is the ordinary Kirchhoff's law, which is not surprising since the condition $A \gg 1$ is equivalent to neglecting the diffusion component of current. Taking into account Eq.(11), we can re-write the last expression in terms of the dimensionless channel conductance $\sigma = jL/(n_c e\mu V_d)$:

$$\sigma = \left[2 \int_0^{1/2} \frac{dt}{1 + g\Psi(t)} \right]^{-1} \quad (17)$$

where

$$g = \frac{2\varepsilon V_g}{\pi e n_c \ln(l/a)} \quad (18)$$

and for $n_c = N$,

$$\Psi(t) = \sum_0^{\infty} \frac{(-1)^n}{(2n+1)} \cos[\pi t(2n+1)] \exp\left[-\frac{\pi d(2n+1)}{L}\right]. \quad (19)$$

The $\sigma(g)$ dependence has a cut-off voltage $g_0 = -\Psi^{-1}(0)$ characterized by vanishing σ and strong increase of $d\sigma/dg$ to the right of g_0 . The exact behavior of these characteristics near the cut-off can be calculated analytically. They are determined by the point of minimal equilibrium concentration, which in a symmetric structure

is $x = 0$, and hence by the properties of $\Psi(t)$ at small t . It can be easily shown that in this region $\Psi(t) \simeq \pi/2 - \arctan[\exp(-\pi d/L)] - (\pi^2 t^2/2) \sinh(\pi d/L) / \cosh^2(\pi d/L)$, which allows us to perform integration in Eq.(17) and obtain

$$\sigma = \frac{\sqrt{(g - g_0) \sinh(\pi d/L)}}{\sqrt{2} \cosh(\pi d/L)},$$

$$g_0 = -\frac{1}{\pi/2 - \arctan[\exp(\pi d/L)]}.$$
(20)

Thus the transconductance $s = d\sigma/dg$ diverges at the cut-off $\sim (g - g_0)^{-1/2}$.

If $n_c \neq N$, the result given by Eq.(20) will not change qualitatively. In this case the function $\Psi(t)$ contains additional contribution from $\phi_c(x)$. This function, studied in more detail in ¹⁰, behaves non-analytically at $x \rightarrow \pm L/2$ but, similarly to $\phi_g(x)$, has an extremum at $x = 0$ and can be expanded in this point. This modifies the value of g_0 and the coefficient in i but retains unchanged the square-root character of $\sigma(g)$ and the divergence of s .

The simplified expressions Eqs.(11),(14),(16),(17) neglected diffusion effects, which is equivalent to the limit of zero temperature. The resulting carrier distribution Eq.(11) does not take into account activation processes and simply gives $n_s = 0$ for all points where $\phi_s^0(x) < -C_t^{-1} n_c$. The potential ϕ_s^0 and the carrier concentration acquire their minimal values at $x = 0$ and, hence, in the linear approximation, the cut-off voltage g_0 corresponds to the condition $\phi_s^0(0) = -C_t^{-1} n_c$ and at lower g the current is exactly zero. At non-zero temperatures the current at $g < g_0$ will have an activation character because of thermal tails of the carrier distribution function: $j \sim \exp(-\Delta/kT)$ where $\Delta = e(-C_t^{-1} n_c - \phi_s^0(0))$ is the barrier height. Since $\phi_s^0(0)$ depends linearly on V_g (see, for instance, Eq.(7)), the activation energy Δ is directly proportional to $g_0 - g$. This means, in turn, that the above-mentioned singularity of $d\sigma/dg$ is fictitious. In fact, its g -dependence will have some maximum at g_0 with a sharp, temperature-dependent decrease at lower g . We do not consider here a tunnelling, though this effect may be important, especially if the carrier effective mass is small, as in the case of a single-wall nanotube. The tunnelling is easily included in a Wentzel-Kramers-Brillouin approximation ¹⁵ (details of the calculation for single-wall nanotubes can be found elsewhere ¹⁶).

5. Current-voltage characteristic of the channel

So far we have dealt with the linear channel conductivity and transconductance at a low source-drain voltage V_d . Another important FET characteristic — the channel current-voltage characteristic (IVC) — and its dependence on the gate voltage and the temperature, can be obtained only by a numerical solution of the Eqs.(2),(3). It is convenient to use dimensionless variables measuring concentrations in units of n_c , lengths in units of L , potentials in units of en_c/ε and current in units of $e^2 n_c^2 \mu / (L\varepsilon)$. The new dimensionless gate potential is related to the parameter g introduced in

Sec.4 as $V_g = (\pi g/2) \ln(l/a)$. For these dimensionless units the basic equation (2) acquires the form

$$j = n(x) \frac{d\phi}{dx} - \left[2 \ln \left(\frac{l}{a} \right) n(x) + \tau \right] \frac{dn}{dx} \quad (21)$$

where $\tau = \varepsilon kT / (e^2 n_c)$ is the dimensionless temperature. The potential consists of three parts: $\phi(x) = \phi_c(x) + \phi_g(x) + \phi_a(x)$ describing the influence of contact work function, gate voltage and source–drain voltage and proportional to $N - n_c$, V_g and V_d , respectively. The particular form of these terms depends on the geometry of contacts and, e.g., for bulk contacts is given by Eqs.(7),(8). The dimensionless version of Eq.(3) for nanotubes can be easily derived from Eq.(21) by assuming $\tau = 0$ and replacing $2 \ln(l/a) \rightarrow \varepsilon C_t^{-1}$.

Eq.(21) should be solved with the two boundary conditions: $n(\pm 1/2) = 1$, which determine the integration constant and the so far unknown value of j . Since $\phi_g(x)$ is proportional to V_g and $\phi_a(x)$ is proportional to V_d , the resulting solution gives us the IVC of a nanowire $j(V_d)$ for various gate voltages.

For our numerical calculations we choose particular values $\ln(l/a) = 3$ and $d/L = 0.3$. Calculations were performed for two situation: ideal Ohmic contacts with $n_c = N$ and undoped nanowire (nanotube) with injecting contacts: $N = 0$.

5.1. Ohmic contacts

In this case the component $\phi_c(x)$ in Eq.(7) is absent and the dimensionless threshold voltage V_{g0} , being estimated with Eq.(20) (that is, in the limit of low temperatures), is equal to -12.8 for our set of parameters. Fig.2 shows IVC at two gate voltages: $V_g = -13.2$ (below the threshold) and $V_g = -12$ (above the threshold). All characteristics have a superlinear character, which has a simple explanation. High driving voltage V_d tends to distribute carriers uniformly along the channel. In our conditions when powerful contact reservoirs fix the concentration n at the points where it is maximal, at the source and the drain, such a re–distribution will increase the minimal value n in the center of channel and hence increase conductivity of the latter. Such superlinear behavior experimentally observed in nanowire–based transistors^{17,18,19,20} differs noticeably from a sublinear dependence typical for both bulk FETs and ballistic nanotube^{21,22,23} structures. We assume that the mechanism of the IVC saturation is due to the contact resistance R_c not included in our theory. When the channel resistance becomes much less than the contact resistance, $R \ll R_c$, almost all the bias drops at the contacts and the current saturates at V_d/R_c .

Fig.2 presents also information on temperature dependence of the channel conductivity. This dependence is practically absent above the threshold. The IVC curves for $V_g = -12$ at different temperatures do not deviate more than by 10% from the dashed line corresponding to a fixed temperature $\tau = 0.2$, and for this reason are not shown in the figure. For V_g below the threshold and for not very large V_d , Fig.2 demonstrates a strong temperature dependence of the current shown

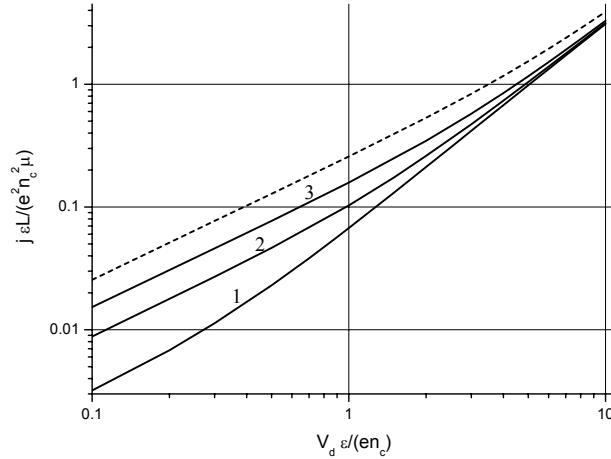


Figure 2: IVC of a 1D FET with $d/L = 0.3$ and Ohmic contacts at different gate voltages: $V_g = -12$ (dashed line) and $V_g = -13.2$ (solid lines) for the temperatures: $\tau = 0.05$ (1); 0.1 (2), and 0.2 (3). (Curves for all three temperatures and $V_g = -12$ coincide.)

in more details in Fig.3. The current is calculated for low $V_d = 0.1$, corresponding to the initial linear part of the IVC. Two upper curves, corresponding to the above-threshold V_g , have no noticeable temperature dependence. In contrast, two lower curves demonstrate such a dependence with the activation energy growing with $|V_g|$, in accordance with the predictions of Sec.4. At high V_d , where contact injection and electric field tend to create uniform carrier concentration equal to n_c , different IVC curves become closer and the temperature dependence collapses.

5.2. Injecting contacts

Though this case formally differs from that considered in the previous subsection, it is only due to the presence of a term $d\phi_c(x)/dx$ in Eq.(21). As it can be seen from Eq.(7), this derivative has singularities at the contacts, which complicates the numerical calculations. To get rid of these singularities, we use the following trick. In the closest vicinity of contacts the first term in the right side of Eq.(21) tends to infinity so that we can neglect the coordinate-independent left side. The remaining terms correspond to a quasi-equilibrium carrier distribution described by Eq.(10) with ϕ_c playing the role of ϕ_s^0 . This formula gives the concentration profile in the vicinity of contacts, which allows us to solve Eq.(21) numerically far from the contact regions and match with this quasi-equilibrium profile as the boundary condition.

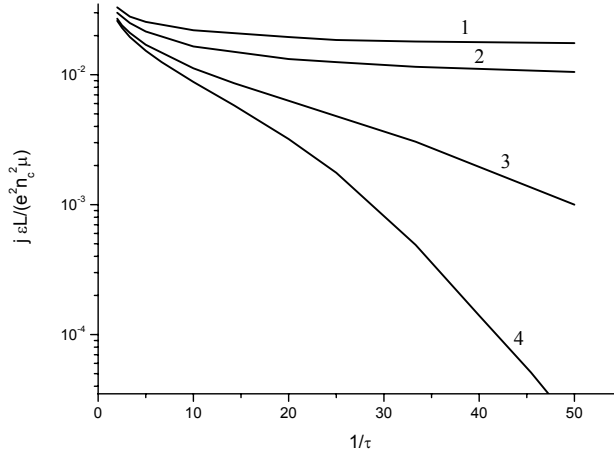


Figure 3: Temperature dependence of the 1D FET conductance in the linear regime ($V_d = 0.1$) for the same device as in Fig.2 at $V_g = -12$ (1); -12.5 (2); -13 (3); -13.2 (4).

Since in our case $\phi_c(x) < 0$ (or, in other words, the electron concentration is lower in the channel due to the absence of doping), we must obtain a lower absolute value of the cut-off voltage and a lower transconductance as compared to the previous subsection. For the same parameters as in Sec.5.1, the cut-off voltage $V_g = -7.64$ as obtained by expanding Eq.(7) near the middle point instead of expression (19) useful only for $n_c = N$. Fig.4 presents the numerical results for the case of injecting contacts. Qualitatively IVCs have the same character as in Fig.2 but a weaker dependence on V_g and the temperature is seen. The above-threshold curve in Fig.5 ($V_g = -6$) is, as in Fig.3, practically temperature-independent (the difference in the currents at $\tau = 0.05$ and $\tau = 0.2$ is less than 5%).

6. The role of contact geometry

6.1. 2D planar contacts

Due to a very weak screening in thin nanowires and nanotubes, the potential profile $\phi^0(x)$ and hence all FET characteristics depend noticeably on the geometry of source and drain contacts^{8,10,30,38}. So far we have considered bulk, three-dimensional contacts (Fig.1A). In many cases contacts to a wire have not bulk but planar character representing highly conducting regions with macroscopic lateral sizes but very small thickness (Fig.1B). In this case the profile of electric field between source and drain

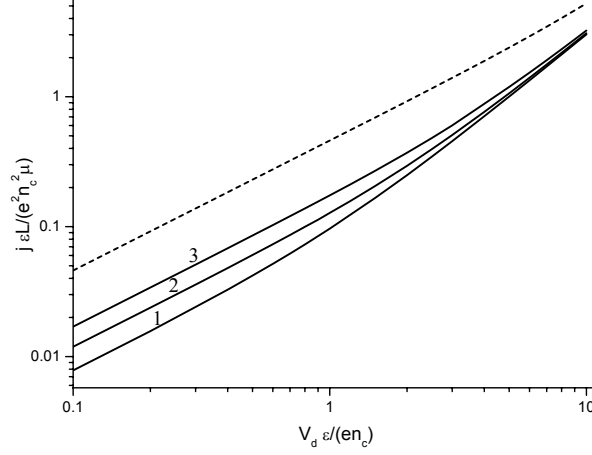


Figure 4: IVC of a 1D FET with $d/L = 0.3$ and injecting contacts at different gate voltages: $V_g = -12$ (dashed line) and $V_g = -13.2$ (solid lines) for the temperatures: $\tau = 0.05$ (1); 0.1 (2), and 0.2 (3). (Curves for all three temperatures and $V_g = -6$ coincide.)

differs drastically from that for bulk electrodes. To confirm this statement, it is enough to remember that in the absence of a gate the electric field between the bulk electrodes is uniform, whereas for the two-dimensional electrodes it has singularities near the contacts.

To find $\phi^0(x)$ in 2D case, we must solve the Laplace equation in the system of coplanar source and drain semi-planes parallel to the gate plane. We split the total potential created by this system, $\Phi(x, y)$, into symmetric and antisymmetric part: $\Phi(x, y) = \Phi_s(x, y) + \Phi_a(x, y)$ and find these parts separately from the Laplace equations with the following boundary conditions:

$$\begin{aligned} \Phi_s(x, 0) &= V_g, & \Phi_s(x > L/2, d) &= 0, & \frac{\partial \Phi_s}{\partial x}(0, y) &= 0; \\ \Phi_a(x, 0) &= 0, & \Phi_a(x > L/2, d) &= V_d/2, & \Phi_a(0, y) &= 0 \end{aligned} \quad (22)$$

and then we find $\phi^0(x) = \Phi(x, d)$.

To solve these problems, we apply the conformal mapping

$$\frac{\pi z}{2d} = \ln(\sqrt{w} + \sqrt{w-1}) + \beta \sqrt{\frac{w-1}{w}} \quad (23)$$

transforming the first quadrant at the $z = x + iy$ plane with the cut $x > L/2, y = d$ into the upper semi-plane at the $w = u + iv$ plane²⁴ so that the source electrode corresponds to the semi-axis $u < 0$, the semi-axis $y > 0$ — to the segment $0 < u < 1$

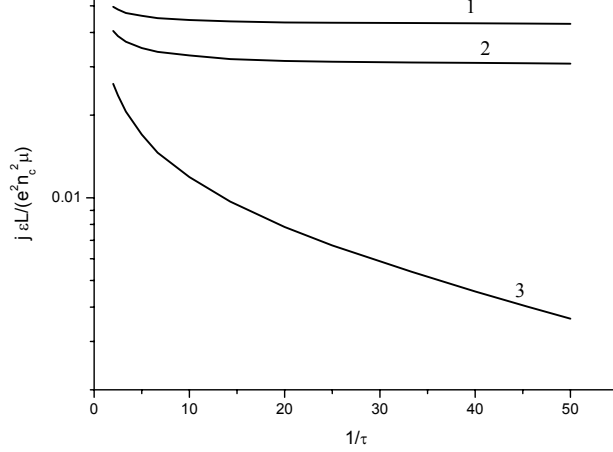


Figure 5: Temperature dependence of the 1D FET conductance in the linear regime ($V_d = 0.1$) for the same device as in Fig.4 at $V_g = -6$ (1); -7.6 (2); -10 (3).

and the gate electrode — to the remaining part of u -axis. The parameter β in Eq.(23) is to be found from the equation

$$\frac{L}{d} = \frac{4}{\pi} \left[\sqrt{\beta(\beta+1)} + \ln \left(\sqrt{\beta} + \sqrt{\beta+1} \right) \right]. \quad (24)$$

It increases monotonically with L/d with the following asymptotes: $\beta \simeq [\pi L/(8d)]^2$ at $L \ll d$ and $\beta \simeq \pi L/(4d)$ at $L \gg d$.

In the (u, v) coordinate system the Laplace equations with the boundary conditions Eq.(22) can be easily solved:

$$\Phi_s(u, v) = V_g \left\{ 1 - \frac{2}{\pi} \operatorname{Im} \left[\ln \left(\sqrt{u+iv} + \sqrt{u+iv-1} \right) \right] \right\}; \quad (25)$$

$$\Phi_a(u, v) = \frac{V_d}{2\pi} \arctan \left(\frac{v}{u} \right). \quad (26)$$

Note that in Eq.(26) the argument of $(\arctan x)$ is in the $(0, \pi)$ interval. These equations along with Eq.(23) determine implicitly the potential profile created by two-dimensional electrodes.

Though we cannot transform analytically the solution Eqs.(25),(26) into the (x, y) coordinate system and obtain $\phi_{s,a}^0(x)$ explicitly, some analytical results could be, nevertheless, obtained. The FET characteristics near the cut-off are determined by the concentration profile $n(x)$ in the vicinity of the minimum of $\phi(x)$. We will perform expansion of $\phi(x)$ in Taylor series near this point. For small V_d this is the point $x = 0$ which means that we need to know only $\phi_s^0(0) \equiv \Phi_s(x=0, y=d)$ and

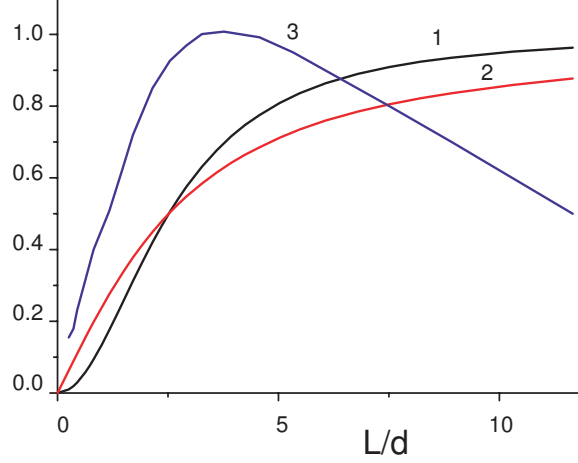


Figure 6: Dependence of (1) the transformation parameter u_0 (see the text), (2) the channel potential $\phi_s^0(0)$ at the minimum and (3) the curvature of the potential $d^2\phi_s^0/dx^2(0)$ on the 1D FET geometry. $\phi_s^0(0)$ is measured in the units of V_g , $d^2\phi_s^0/dx^2(0)$ — in the units of $2V_g/L^2$.

the second derivative of ϕ_s^0 in this point. In (u, v) coordinates the above-mentioned point is $(u_0, 0)$ where $0 < u_0 < 1$ and is determined by the equation

$$\arctan \sqrt{\frac{1-u_0}{u_0}} + \beta \sqrt{\frac{1-u_0}{u_0}} = \frac{\pi}{2}. \quad (27)$$

Fig.6 shows the dependence of u_0 on the parameter L/a obtained from Eqs.(24),(27) and having the following asymptotes: $u_0 \simeq [\pi L/(8d)]^2$ at $L \ll d$ and $u_0 \simeq 1-4d^2/L^2$ at $L \gg d$. By substituting this u_0 and $v = 0$ into Eq.(25) we obtain $\phi_s^0(0)$ also shown in a Fig.6. It has the asymptotes: $\phi_s^0(0) \simeq V_g L/(4d)$ at $L \ll d$ and $\phi_s^0(0) \simeq V_g[1-4d/(\pi L)]$ at $L \gg d$. The curvature $d^2\phi_s^0/dx^2(x=0)$ was also calculated and presented at the same figure.

6.2. 1D wire-like contacts

It is appealing to fabricate the contacts to the 1D channel in the form of two thin wires perpendicular to the channel (see, e.g., ²⁵). This is geometry of a 1D contact as it is shown in Fig.1C. If we assume these wires to be infinitely long (which means that their length considerably exceeds L) and have the radius a_c , then the potentials can be calculated relatively simply as the sum of potentials created by 4 cylinders (source, drain and their images in the backgate):

$$\phi_s(x) = V_g + \frac{V_g}{\ln(L/a_c)} \ln \frac{(x+L/2+a_c)(-x+L/2+a_c)}{\sqrt{4d^2+(x+L/2)^2}\sqrt{4d^2+(-x+L/2)^2}}; \quad (28)$$

$$\phi_a(x) = \frac{V_d}{2 \ln(L/a_c)} \ln \frac{(x + L/2 + a_c) \sqrt{4d^2 + (x + L/2)^2}}{(-x + L/2 + a_c) \sqrt{4d^2 + (-x + L/2)^2}}. \quad (29)$$

Calculations of the transconductance in the linear regime are based on the same formula Eq.(17) as in the Sec.4. The quantitative difference is in a particular profile of the $\Psi(t)$ function. Though its expansion near the maximum is, of course, also quadratic and hence it gives qualitatively the same final result $di/dg = A(g - g_0)^{-1/2}$, the expansion coefficients are different. As a result, the cut-off voltage g_0 and the coefficient A may differ considerably from the case of bulk contacts. The whole IVC, as before, must be found by numerical calculations taking into account the fact that for two-dimensional contacts not only $\phi_c(x)$ but also $\phi_g(x)$ have singularities near the contacts. Thus one has to match the numerical solution in the middle of the channel with an analytical quasi-equilibrium solution in the region near the contacts as described in Sec.5.2, even for the Ohmic contacts.

7. Hysteresis and memory effects

The theoretical model considered in the previous sections gives a general physical picture and qualitative regularities describing electrical parameters of 1D FETs but, being general, cannot account for all specific features observed experimentally. For instance, some recent studies^{26,27,28} demonstrated that IVCs of nanotube-based FETs have a strong hysteretic effect revealed as a difference in the threshold gate voltages measured for V_g swept in positive and negative direction. A similar hysteresis is known to exist for Si devices and exploited for the memory elements²⁹. By analogy, it was supposed that these nanotube FETs may also become nonvolatile memory elements operating at the few-(single-)electron level even at elevated temperatures. In Si devices hysteresis is usually explained by generation/recombination of electrons at the traps in the oxide layer (the so-called slow surface states). In our case, we may expect a similar recharging stimulated by the channel-gate electric field (the Fowler-Nordheim effect). This field in quasi-1D-systems is $\sim a^{-1}$ in the vicinity of channel and, hence, can be very high. One may therefore expect the memory effects to be observed at lower V_g , as compared to classical FETs. The described electron tunnelling to (or from) dielectric layer causes potential redistribution in the system resulting in a shift of the threshold voltage. Due to a low tunnelling probability, the characteristic time of corresponding charge transport may exceed the inverse frequency of V_g sweeping, which is consistent with the observed hysteresis.

For further phenomenological description we assume that the distribution of this charge is cylindrically symmetric. For FET model with a cylindrical gate (see, e.g.,³⁰) it is definitely the case. Moreover, we may expect this assumption to be also correct even in the planar gate geometry discussed in the previous sections if the nanotube/nanowire is completely buried in the oxide. According to the general expressions of Sec.2, we can claim that the shift of threshold voltage due to recharging of traps in the dielectric

$$\delta V_{g0} = \frac{e\delta N(0)}{C_t}, \quad (30)$$

where $\delta N(0)$ is the linear density of such charged traps taken at $x = 0$ since this point plays the role of a 'bottleneck' determining the offset of channel current.

The value of $\delta N(0)$ is found from the generation-recombination equation describing recharging of traps through the Fowler-Nordheim mechanism. If the maximal possible $\delta N(0)$ is limited by the total density of empty traps in a thin shell accessible for tunnelling electron, N_0 ,[‡] then its dynamics is dictated by the equation

$$\frac{d\delta N(0)}{dt} = \frac{J\sigma}{e} [N_0 - \delta N(0)]. \quad (31)$$

Here $\sigma \simeq 10^{-17} \text{ cm}^2$ is the cross-section of the generation (and recombination)³¹, and we estimate $N(0) = 10^{13} \text{ cm}^{-2}$ ³³. The Fowler-Nordheim current density depends on the electric field near the FET channel \mathcal{E} , which in turn depends on the potential and the radius of the 1D channel R (and logarithmically depends on the gate distance d): $\mathcal{E} = \phi/(R \ln(d/2R))$.

$$J = A\phi^2 \exp(-B/\phi) \quad (32)$$

where the constants $A \simeq 10^5 \text{ A cm}^{-2} \text{ V}^{-2}$ and $B \simeq 150 \text{ V}$ are known for tunnelling in typical materials³² and depend mostly on the effective mass of the carriers and the trap level.

Eq.(32) has been solved numerically and the result depends on the sweeping rate (SR) and the sweeping range of V_g that reflect the specifics of a particular experiment with a nanotube or nanowire FET. The physics of this dependence is clear: the slower V_g is swept and the larger is the sweeping range, the larger the density of injected electrons (cumulative charge in the substrate in our case), and thus the larger the hysteresis in accord with Eq.(30). The results of our modelling are presented in Fig.7. The potential of the ionized impurities creates an additional term (30) in the external potential as given by Eq.(7). This term is plotted in the figure as a function of the gate voltage. This extra term shifts the threshold voltage as given by expression (20). The shift is different for different direction of the gate voltage sweep, because the traps are charged/discharged when the voltage is swept up/down.

The dependence of the hysteresis width, H , on the sweeping rate is close to logarithmic. We explain this by the exponential dependence of the steady state solution of the Eqs. (31,32) on the electrostatic potential, then, the potential itself is roughly proportional to the $\log \delta N$ which is proportional in turn to the sweeping rate. Similarly, the hysteresis increases with the sweeping range as shown in Fig.8.

[‡]For large N_0 , the maximal $\delta N(0)$ can be limited not by the absence of empty traps but by the drop of the local channel-gate electric field making the tunnelling rate too small to be observed in real time.

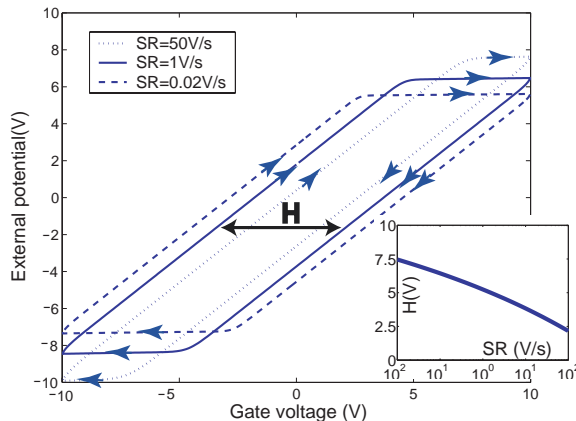


Figure 7: The potential induced by ionized traps vs. the sweeping rate of V_g . Inset: log-linear plot of the hysteresis width, H , vs the sweeping rate.

Following the theory of Sec.4, we can write the FET drive current density in a linear regime via the integral of the inverse quasi-equilibrium charge density, Eq.(16). Since in this section we are mostly interested in describing the effect of the hysteresis, for clarity of the presentation, we apply a toy model with the full axial symmetry of the cylindrical gate and trap potential. This approximation may though give a realistic estimate for the device with planar gate geometry which was discussed in the rest of the paper. This is because the transport at the threshold mostly depends on the potential profile at the middle of the channel, where it is almost flat. We note that in this model the effects of the fringe fields at the channel ends and all contact phenomena are fully neglected.

If all potentials have full cylindrical symmetry, the integration along the channel length is trivial and gives for the driving current density:

$$j = V_d \frac{\epsilon \mu}{L} (n_c + \Delta n_0(x)). \quad (33)$$

where $\mu = 9000 \text{ cm}^2/\text{Vs}$, $d = 500 \text{ nm}$ and $L = 10d = 5 \mu\text{m}$ is the effective length of the FET channel (the length over which the potential can be considered flat within the cylindrical model). We conclude that in the cylindrical gate model, the current in the linear regime is a linear function of the channel charge density as in a standard MOSFET. Substituting the parameters as specified above, we obtain the IVCs, shown in Fig.9.

8. Conclusions

The present work is devoted to the theory of nanowire and nanotube based transistor structures, which represents an important step towards developing a general theory of nanoscale 1D devices. In the framework of our problem we model a carrier

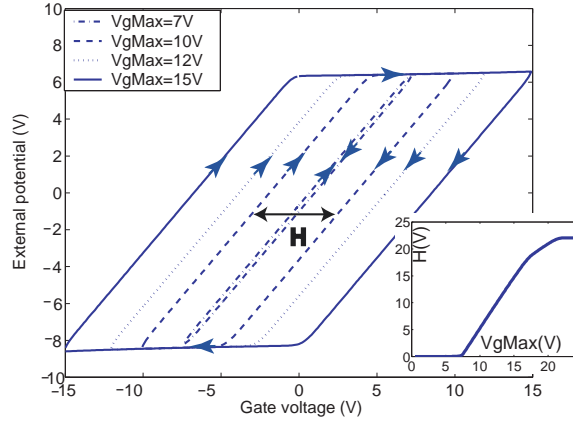


Figure 8: The potential induced by ionized traps vs. the sweeping range (at the sweeping rate 0.1 V/s). Inset: Hysteresis width vs. the sweeping range.

distribution and a conductivity in a quasi-1D channel placed between two metal electrodes over a backgate electrode. This structure is in fact a 1D FET. For details on the fabrication and experimental investigation of nanowire FETs in the recent years we refer to publications ^{18,20,34}. To give an adequate theoretical description of basic characteristics of a 1D FET is the main task of our calculation. These results, with some restrictions, can be applied to such important object as a carbon nanotube FET ^{22,35,36}. The mentioned restrictions are due to the fact that we treat the carrier motion in a channel within a drift-diffusion model while short carbon nanotubes are believed to have a ballistic conductivity ^{8,13,37}. That is why the universal nanowire and nanotube model presented above is presumably applicable to the nanotube devices with a long enough channel only. We note that our theory in the part related to the induced potential profile is still applicable to any 1D device which is at the equilibrium (or very close to it) because the calculation of the equilibrium charge distribution does not depend on any assumption about the charge transport mechanism.

We focus in this paper on a universal analytical solution for the transport equations in a 1D channel under the drift-diffusion approximation, which has not been formulated previously. An essential difference for the 1D-FET model as compared with a standard planar FET model is due to the poor screening at the low dimensions. Thus, the channel resistance, which is shown to depend on the self-consistent charge density in the channel, can be more effectively controlled by the gate voltage. Although the operation principle of the 1D-FET is similar to the planar device, different electrostatics for the 1D channel results in a different behavior and in different device characteristics. For example, the transconductance at the threshold, unlike in a bulk FET, has a typical dependence $\sim 1/\sqrt{V_g - V_{g0}}$. With a lower (leakage) OFF currents observed recently in 1D-FET, this makes these devices very attractive

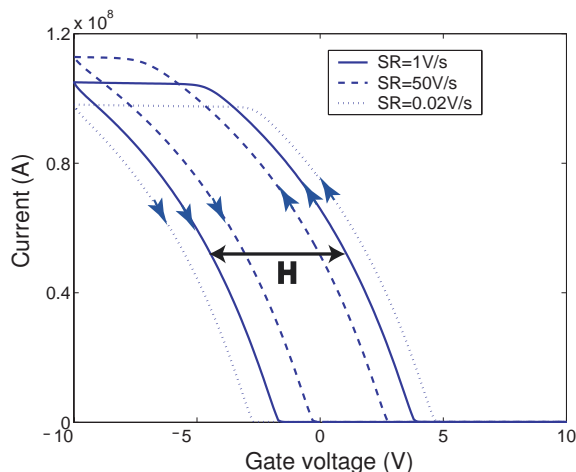


Figure 9: Current (in neglecting the contact resistance) vs. the gate voltage for different sweeping rates: 0.02, 1 and 50 V/s.

for electronic applications.

We have shown above that our transport model may have a straightforward generalization to a case of existence of movable/ionizable charges placed around the channel. This problem has a direct relevance for nanotube FETs and for a few of nanowire devices (to be discussed elsewhere). The model of the hysteresis, responsible for the memory effects in nanotube FETs, is presented. We calculated the typical IVCs taking into account the generation/recombination at the charge traps within a simple toy model (of a cylindrical gate) for an effective channel resistance. We note that a similar approach describes adequately the 1D FET with a chemically or bio-functionalized channel (to be published elsewhere).

Acknowledgments

S.V.R. acknowledges partial support by start-up fund and Feigl Scholarship of Lehigh University, the DoE grant DE-FG02-01ER45932 and the NSF grant ECS-04-03489.

1. S.V. Rotkin, H.E. Ruda, and A. Shik, "Universal Description of Channel Conductivity for Nanotube and Nanowire Transistors", *Appl. Phys. Lett.* **83** (2003) 1623–1625.
2. T. Ando, A.B. Fowler, and F. Stern, "Electronic properties of two-dimensional systems", *Rev. Mod. Phys.* **52** (1982) 437–672.
3. N.S. Averkiev and A.Y. Shik, "Contact phenomena in quantum wires and porous silicon", *Semiconductors* **30** (1996) 112–116.
4. A. Robert-Peillard, S.V. Rotkin, "Modeling Hysteresis Phenomena in Nanotube Field-Effect Transistors", *IEEE Transactions on Nanotechnology*, accepted, (2004).
5. P.S. Carney, Y. Li, and S.V. Rotkin, "Probe functions in near-field microscopy with single-wall nanotubes", submitted, 2005.

6. S.V. Rotkin, "Theory of Nanotube Nanodevices", in *Nanostructured Materials and Coatings for Biomedical and Sensor Applications*, (Proceedings of the NATO Advanced Research Workshop; August 4–8, 2002, Kiev, Ukraine). Editors: Y.G. Gogotsi and Irina V. Uvarova. Kluwer Academic Publishers: Dordrecht–Boston–London. NATO Science Series: II. Mathematics, Physics and Chemistry — Vol. 102, pp. 257–277, (2003).
7. D. Lu, Y. Li, S.V. Rotkin, U. Ravaioli, and K. Schulten, "Wall Polarization in a Carbon Nanotube Water Channel", *Nano Lett.*, 4(12), (2004) 2383–2387. For an experimental work, see N. Naguib, H. Ye, Y. Gogotsi, A.G. Yazicioglu, C.M. Megaridis, and M. Yoshimura, "Observation of Water Confined in Nanometer Channels of Closed Carbon Nanotubes" *Nano Lett.*, 4(11), (2004) 2237–2243.
8. S. Heinze, J. Tersoff, R. Martel, V. Derycke, J. Appenzeller, and Ph. Avouris, "Carbon Nanotubes as Schottky Barrier Transistors" *Phys. Rev. Lett.* **89** (2002) 106801–106804.
9. A.G. Petrov, S.V. Rotkin, "Transport in Nanotubes: Effect of Remote Impurity Scattering", *Phys. Rev. B* vol. 70 no. 3 (2004) 035408–1–10.
10. H. Ruda and A. Shik, "Influence of contacts on the conductivity of thin wires", *J. Appl. Phys.* **84** (1998) 5867–5872.
11. K.A. Bulashevich and S.V. Rotkin, "Nanotube Devices: Microscopic Model", *JETP Lett.* **75**(2002) 205–209.
12. S.V. Rotkin, V. Srivastava, K.A. Bulashevich, and N.R. Aluru, "Atomistic Capacitance of a Nanotube Electromechanical Device", *Int. J. Nanosci.* **1** (2002) 337–346.
13. T. Nakanishi, A. Bachtold, and C. Dekker, "Transport through the interface between a semiconducting carbon nanotube and a metal electrode", *Phys. Rev. B* **66**, (2002) 073307–073310.
14. M. Abramowitz and L. Stegun, *Handbook of Mathematical Functions with Formulas, Graphs, and Mathematical Tables*, (Academic Press, 1975).
15. L.D. Landau, E.M. Lifshits. *Quantum Mechanics*, (Pergamon, Oxford, 1984).
16. S.V. Rotkin, "Theory of Nanotube Opto-electromechanical Device", Proceedings of Third IEEE conference on Nanotechnology, 12–14 August 2003. Moscone Convention Center, San-Francisco, CA. pp. 631–634.
17. T. Maemoto, H. Yamamoto, M. Konami, A. Kajiuchi, T. Ikeda, S. Sasa, and M. Inoue, "High-speed quasi-one-dimensional electron transport in InAs/AlGaSb mesoscopic devices", *Phys. Stat. Sol. (b)* **204** (1997) 255–258.
18. Y. Cui, X. Duan, J. Hu, and C. M. Lieber, "Doping and electrical transport in silicon nanowires", *J. Phys. Chem. B* **104** (2000) 5213–5216.
19. G. L. Harris, P. Zhou, M. He, and J. B. Halpern, "Semiconductor and photoconductive GaN nanowires and nanotubes", *Lasers and Electro-Optics, 2001, CLEO'01*. Technical Digest, p.239.
20. J.-R. Kim, H. M. So, J. W. Park, J.-J. Kim, J. Kim, C. J. Lee, and S. C. Lyu, "Electrical transport properties of individual gallium nitride nanowires synthesized by chemical-vapor-deposition", *Appl. Phys. Lett.* **80** (2002) 3548–3550.
21. X. Liu, C. Lee, and C. Zhou, "Carbon nanotube field-effect inverters", *Appl. Phys. Lett.* **79** (2001) 3329–3331.
22. S. J. Wind, J. Appenzeller, R. Martel, V. Derycke, and P. Avouris, "Vertical scaling of carbon nanotube field-effect transistors using top gate electrodes", *Appl. Phys. Lett.* **80** (2002) 3817–3819.
23. F. Leonard and J. Tersoff, "Multiple Functionality in Nanotube Transistors", *Phys. Rev. Lett.* **88** (2002) 258302–258305.
24. W. von Koppenfels and F. Stallmann, *Praxis der konformen Abbildung*, (Springer-Verlag, 1959).

25. J.-F. Lin, J.P. Bird, L. Rotkina, and P.A. Bennett, “Classical and quantum transport in focused-ion-beam-deposited Pt nanointerconnects”, *Appl. Phys. Lett.* **82** (2003) 802–804.
26. M. Radosavljevic, M. Freitag, K. V. Thadani, and A. T. Johnson, “Nonvolatile Molecular Memory Elements Based on Ambipolar Nanotube Field-Effect Transistors”, *Nano Letters*, v.2 (2002) 761–764.
27. M. S. Fuhrer, B. M. Kim, T. Durkop, and T. Brintlinger, “High Mobility Nanotube Transistor Memory”, *Nano Letters*, v.2 (2002) 755–759.
28. W. Kim, A. Javey, O. Vermesh, Q. Wang, Y. Li, and H. Dai, “Hysteresis Caused by Water Molecules in Carbon Nanotube Field-Effect Transistors”, *Nano Letters*, v.3 (2003) 193–198.
29. L. Guo, E. Leobandung, and S.Y. Chou “A Silicon Single-Electron Transistor Memory Operating at Room Temperature”, *Science* 275 (1997) 649–651.
30. A. Odintsov and Y. Tokura, “Contact Phenomena and Mott Transition in Carbon Nanotubes”, *Journal of Low Temp. Physics*, v.118, no 5–6 (2000) 509–518.
31. Y. Roh, L. Trombetta, J. Han, “Analysis of Charge Components Induced by Fowler-Nordheim Tunnel Injection in Silicon Oxides Prepared by Rapid Thermal Oxidation”, *J. Electrochem. Soc.*, v.142 (1995) 1015–1020.
32. P.T. Landsberg, *Recombination in semiconductors*, (Cambridge, 1991).
33. M. Fischetti, R. Gastaldi, F. Maggioni, and A. Modelli, “Positive charge effects on the flatband voltage shift during avalanche injection on Al-Si O₂-Si capacitors,” *J. of Appl. Phys.*, vol. 53 (1982) 3129–3136.
34. H. Hasegawa and S. Kasai, “Hexagonal binary decision diagram quantum logic circuits using Schottky in-plane and wrap-gate control of GaAs and InGaAs nanowires”, *Physica E* **11**, no. 2–3 (2001) 149–154.
35. S. J. Tans, A. R. M. Verschueren, and C. Dekker, “Room-temperature transistor based on a single carbon nanotube”, *Nature* **393** (1998) 49–52.
36. R. Martel, T. Schmidt, H. R. Shea, T. Hertel, and P. Avouris, “Single- and multi-wall carbon nanotube field-effect transistors”, *Appl. Phys. Lett.* **73** (1998) 2447–2449.
37. J. Guo, M. Lundstrom, and S. Datta, “Performance projections for ballistic carbon nanotube field-effect transistors”, *Appl. Phys. Lett.* **80** (2002) 3192–3194.
38. Authors are grateful to an Anonymous Reviewer for calling our attention to the reference: J. Guo, J. Wang, E. Polizzi, S. Datta, and M. Lundstrom, “Electrostatics of nanowire transistors”, *IEEE Trans. on Nanotechnology* **2** (2003) 329–334, which paper further applies results of ³⁰ and ¹¹ to a specific device geometry.